Real-time probing of chirality during a chemical reaction

Denitsa Baykusheva[a], Daniel Zindel[a], Vít Svoboda[a], Elias Bommeli[a], Manuel Ochsner[a], Andres Tehlar[a], and Hans Jakob Wörner[a,1]

[a]Laboratory of Physical Chemistry, ETH Zürich, 8093 Zürich, Switzerland

Edited by Alexis T. Bell, University of California, Berkeley, CA, and approved October 16, 2019 (received for review April 29, 2019)

Chiral molecules interact and react differently with other chiral objects, depending on their handedness. Therefore, it is essential to understand and ultimately control the evolution of molecular chirality during chemical reactions. Although highly sophisticated techniques for the controlled synthesis of chiral molecules have been developed, the observation of chirality on the natural femtosecond time scale of a chemical reaction has so far remained out of reach in the gas phase. Here, we demonstrate a general experimental technique, based on high-harmonic generation in tailored laser fields, and apply it to probe the time evolution of molecular chirality during the photodissociation of 2-iodobutane. These measurements show a change in sign and a pronounced increase in the magnitude of the chiral response over the first 100 fs, followed by its decay within less than 500 fs, revealing the photodissociation to achiral products. The observed time evolution is explained in terms of the variation of the electric and magnetic transition-dipole moments between the lowest electronic states of the cation as a function of the reaction coordinate. These results open the path to investigations of the chirality of molecular-reaction pathways, light-induced chirality in chemical processes, and the control of molecular chirality through tailored laser pulses.

chirality | high-harmonic generation | circular dichroism | ultrafast chirality | femtochirality

The two enantiomers of a chiral molecule interact differently with chiral receptors and with chiral light. The former effect is the basis of chiral recognition, an essential mechanism of biomolecular function. The latter is the principle of optical techniques for detecting chirality. Although extensive control over molecular chirality has been achieved in enantio-selective synthesis of molecules (1–3), chiral sensitivity has been lacking from all femtosecond time-resolved probes of chemical reactions in the gas phase demonstrated to date. The main origin of this shortcoming is the weakness of chiral light–matter interactions, which rely on magnetic-dipole, electric-quadrupole, and higher-order interactions. For this reason, circular dichroisms (CDs) in absorption spectroscopies are typically very weak effects in the range of 10^{-6} to 10^{-3} relative signal changes. Nevertheless, time-resolved CD (TRCD) techniques have gained increasing attention over the last 15 y (4) and nowadays cover the infrared (5, 6), visible (7), and ultraviolet (UV) (8–11) spectral regions. The promise of extending such measurements to the X-ray domain has recently been predicted (12–14). Unfortunately, the inherent weakness of the optical CD effects and the related technical challenges have so far limited TRCD measurements to the condensed phase and to picosecond or longer time scales.

The development of more sensitive methods, applicable to isolated molecules in the gas phase, has therefore received considerable attention (15). Important developments include microwave three-wave-mixing spectroscopy (16), Coulomb explosion imaging (17, 18), laser-induced mass spectrometry (19, 20), photoelectron CD [PECD (21–25)], and high-harmonic generation (HHG) in weakly elliptically polarized one-color (26) and elliptically to circularly polarized two-color laser fields (27). Whereas the former technique still yields very low chiral discrimination, the latter has been shown to achieve up to 13% chiral discrimination (27). Time-resolved PECD (TR-PECD) has so far only been demonstrated in the single-photon-ionization regime by using laser pulses in the visible domain (28). As a consequence, it has remained restricted to probing dynamics in highly excited states rather than photochemical reactions. The extension of TR-PECD to extreme UV and soft-X-ray radiation derived from high-harmonic and X-ray free-electron laser facilities currently represents an active research direction.

Here, we introduce an all-optical, ultrafast, and nearly general experimental technique for probing the time-dependent chirality of molecules undergoing a photochemical reaction. This method combines the established sensitivity of HHG spectroscopy to photochemical dynamics (29–31) with the unique chiral sensitivity of HHG in two-color counterrotating circularly polarized (so-called "bicircular") laser fields, which was theoretically predicted (32–34) and experimentally demonstrated on unexcited molecules very recently (27, 35).

The key advantages of our pump–probe technique are its sensitivity to gas-phase samples, its temporal resolution, and the background-free detection of the excited-state dynamics. We demonstrate the ability of the technique to follow in real time the evolution of molecular chirality along a photochemical reaction pathway. This development paves the way to detecting the chiral interactions that underlie enantio-specific chemical

Significance

Chiral molecules interact and react differently, depending on their handedness (left vs. right). This chiral recognition is the principle governing most biomolecular interactions, such as the activity of drugs or our perception of scents. In spite of this fundamental importance, a real-time (femtosecond) observation of chirality during a chemical reaction has remained out of reach in the gas phase. In the present work, we report this breakthrough with a seemingly unlikely technique: high-harmonic generation (HHG) in tailored intense near-infrared laser fields. Combining the transient-grating technique with HHG in counterrotating circularly polarized laser fields, we follow the temporal evolution of molecular chirality during a chemical reaction from the unexcited electronic ground state through the transition-state region to the final achiral products.

Author contributions: H.J.W. designed research; D.B., V.S., and A.T. performed research; D.Z., V.S., E.B., M.O., and A.T. contributed new reagents/analytic tools; D.B. analyzed data; and D.B. and H.J.W. wrote the paper.

The authors declare no competing interest.

This article is a PNAS Direct Submission.

[1]To whom correspondence may be addressed. Email: hwoerner@ethz.ch.

This article contains supporting information online at www.pnas.org/lookup/suppl/doi:10.1073/pnas.1907189116/-/DCSupplemental.

reactions. Building on the self-probing capabilities of high-harmonic spectroscopy (36, 37), our technique also provides access to the attosecond electron dynamics (38) of the underlying chiral response (27) and its dependence on the chemical-reaction pathway. With the recent extensions of high-harmonic spectroscopy to solids (39–41) and liquids (42), our technique will rapidly become applicable to all phases of matter. In the liquid phase, it will give access to the interactions underlying chiral recognition. In the solid state, it might open approaches to elucidate dynamics in chiral crystals, such as chiral magnetic or magnetoelectric effects. Its all-optical nature paired with its high degree of chiral discrimination will facilitate its application to dense or highly charged forms of matter.

Results

The light-induced dissociation of 2-iodobutane ($2-C_4H_9I$), depicted in Fig. 1, was selected as an illustrative chemical reaction. Photoexcitation of this molecule at 266 nm accesses the $\tilde{A}$ band and mainly populates the $^3Q_0^+$ state in a parallel transition, as revealed by magnetic CD measurements (43). The repulsive potential-energy curves of the $^3Q_0^+$ and the two close-lying electronic states ($^3Q_1$ and $^1Q_1$) are given in *SI Appendix*, Figs. S3 and S4. Following excitation to the $^3Q_0^+$ state, the molecule dissociates into a 2-butyl radical and a spin-orbit–excited iodine atom (I^*, $^2P_{1/2}$) on an ultrafast time scale.

The breakage of the C–I bond also induces a major modification of the chiral structure of the molecule. The main idea of our work is to map out the temporal evolution of the molecular chirality as the laser-induced photodissociation takes its course. We thereby answer the following questions. Is the 2-butyl radical produced in a chiral or achiral state? How fast do the signatures of the changing chirality evolve from the reactant to the product state? Which properties of molecular chirality is our method sensitive to?

The experimental setup is illustrated in Fig. 2. A transient grating [TG (29, 30, 44)] was produced by crossing two linearly polarized, vertically offset 266-nm pulses in a supersonic expansion of gaseous 2-iodobutane. A periodic intensity-variation pattern was produced in the focal plane, and, as efficient photoexcitation was restricted to the high-intensity regions, this modulation translated into alternating planes of excited and ground-state molecules. The TG was probed by a bicircular field consisting of the superposition of 2 circularly polarized ∼40-fs pulses centered at 1,800 and 900 nm, respectively, with opposite helicities. The corresponding electric field describes a Lissajous figure resembling a clover leaf, as illustrated in Fig. 2, *Left*. As the HHG radiation emitted from the individual layers of the grating in the near field is characterized by different amplitudes and phases, a diffraction pattern is formed in the far field, leading to a background-free detection of the excitation (*SI Appendix*, Fig. S1). As revealed by the data presented in *SI Appendix*, the typically achieved diffraction efficiencies reached up to 7 to 8%.

The experiment consisted of measuring the intensity of the diffracted and undiffracted high-harmonic emission as a function of the time delay between the excitation and probe pulses. The dynamics of the 2-iodobutane photodissociation were investigated for pump–probe delays Δt spanning the range from -0.15 to 5 ps. Fig. 2, *Lower Right* shows the short-time evolution of signal in harmonic order 23 ([H23] of 1,800 nm, ~ 15.8 eV) recorded in racemic 2-iodobutane. The orange curve represents the undiffracted intensity ($I_{m=0}$), while the averaged diffracted ($m=\pm 1$) signals are shown in dark green. Temporal overlap of the pump and probe pulses led to high-order wave mixing (45), which appeared spatially separated from the other signals on the detector (*SI Appendix*, Fig. S1). This wave-mixing signal, averaged over its two components ($wm=\pm 1$), is shown as black line. It accurately determines the characteristic cross-correlation time of the experiment (≈ 45 fs).

The temporal evolution of the undiffracted intensities is qualitatively similar for all harmonic orders, as is the time evolution of all observed diffracted intensities. We characterized the photodissociation dynamics observed in each harmonic order by quantifying the exponential time scale of intensity buildup in the diffracted signals τ_{rise}, defined by the phenomenological kinetic expressions given in *SI Appendix*, Eqs. S1 and S2. The extracted values of τ_{rise}, averaged over multiple measurements, are listed in *SI Appendix*, Table I. Notably, the observed (averaged) dissociation time scale ($\tau_{\mathrm{rise}} \approx 340$ fs) is longer than the estimations from wave-packet calculations (*SI Appendix*, section IV) or extrapolations from previous studies (see discussion in ref. 46). This observation is in line with the conclusions from previous TG-HHG studies on the photodissociation dynamics of Br_2 (29) and other alkyl halides employing linearly polarized driving fields (47).

We now turn to the characterization of the time-dependent chirality during the photodissociation. Enantiomerically enriched samples ($ee \sim 60-65\%$) of (R)- and (S)-2-iodobutane were synthesized in-house as described in *SI Appendix*, section II. The chirality sensitive measurements were performed by monitoring the signal of the undiffracted emission ($I_{m=0}$) as the ellipticity of the ω and 2ω laser fields constituting the bicircular field is varied by rotating the main axis of the achromatic quarter waveplate (QWP) from $\alpha = 30^\circ$ to $\alpha = 150^\circ$. In this manner, the polarization of the ω and 2ω laser fields is changed from circular via elliptical to linear and then back to circular again (with opposite helicity). At both $\alpha = 45^\circ$ and $\alpha = 135^\circ$, the two pulses combined into a bicircular field, but with opposite helicities. These two helicities interact differently with the chiral molecules, resulting in a CD effect in the intensity of the emitted high-harmonic radiation. *SI Appendix*, section IC

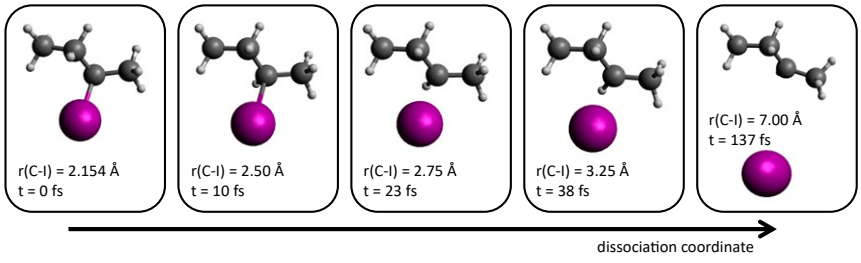

Fig. 1. Illustration of the investigated photochemical reaction. An initially chiral molecule is photoexcited by a femtosecond laser pulse centered at 266 nm. The ensuing photodissociation reaction leads to a time-dependent change in the chiral structure of the molecule. The leftmost image displays the equilibrium geometry of (*R*)-2-iodobutane (see *SI Appendix* for details). The structures in the other images have been obtained by varying the C–I bond distance and relaxing all remaining degrees of freedom. The corresponding time delays have been taken from the wave-packet calculations shown in *SI Appendix*, Fig. S12.

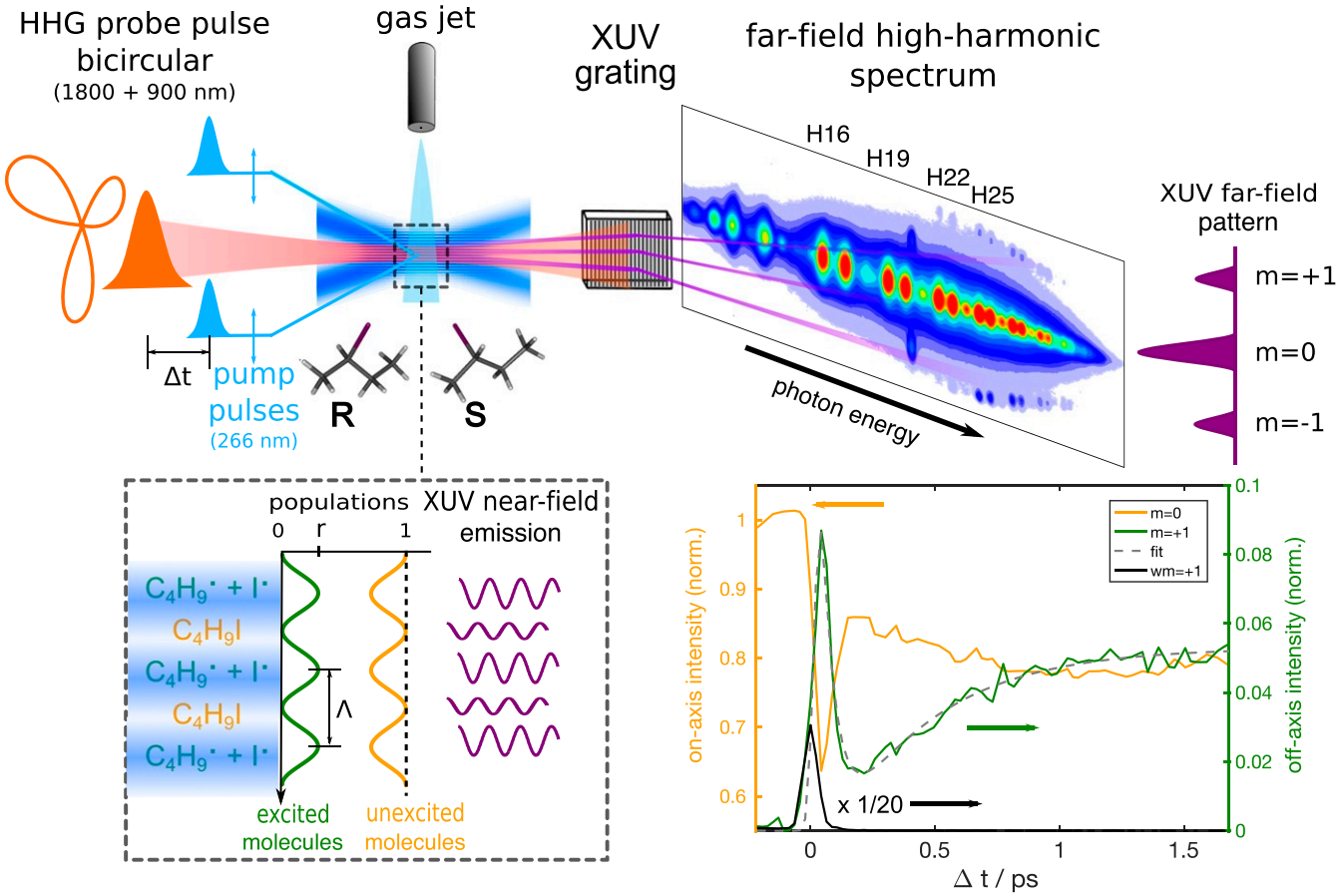

Fig. 2. Principle of bicircular high-harmonic transient-grating spectroscopy. Two noncollinear pump beams are crossed under a small angle, creating an intensity grating which spatially modulates the molecular excitation. High-harmonic radiation is generated by a temporally delayed bicircular field consisting of a 1,800-nm pulse and its second harmonic centered at 900 nm. In the far field, the radiation diffracted by the optical grating is spatially separated from the undiffracted light. *Lower Right* shows the time-dependent signals observed in 2-iodobutane after excitation at 266 nm followed by HHG driven by a bicircular 1,800 + 900-nm field observed in the undiffracted orders (orange curve, left-hand vertical axis) and averaged $wm = \pm 1$ (black) and $m = \pm 1$ (dark green) orders (left-hand axis) for harmonic 23 of 1,800 nm ($\sim$ 15.8 eV). The origin of the time scale has been set to the maximum of the wave-mixing signal. norm., normalized; XUV, extreme UV.

outlines the procedure for extracting the frequency- and ellipticity-dependent CD $CD(n\omega, \alpha)$ from the normalized HHG intensities $I_{R/S}(n\omega)$ recorded from each enantiomer, where $n\omega$ denotes the frequency of the n^{th} harmonic of the fundamental frequency ω. We further define an ellipticity-averaged quantitative measure for the observed CD by averaging the ellipticity-resolved $CD(n\omega, \alpha)$ in the region close to the two opposite bicircular configurations ($\alpha \in [35^\circ - 55^\circ]$, respectively $\alpha \in [125^\circ - 145^\circ]$):

$$\overline{CD}^{\pm}(n\omega) = \int_{\alpha_{\min}}^{\alpha_{\max}} CD(n\omega, \alpha) \mathrm{d}\alpha, \qquad [1]$$

whereby the superscript $\pm$ specifies the 2 possible helicity combinations of the ω and 2ω laser fields. This procedure minimizes the asymmetries resulting from imperfections of the optical components and the optical path misalignments and expresses the CD as a function of the photon energy only.

Fig. 3 shows the high-harmonic signal in H19 in terms of the undiffracted-signal intensities emitted from the individual enantiomeric samples [(*R*) and (*S*)] as blue and red curves in *Upper*. The differential ellipticity-resolved CDs are shown in *Lower*. Since the two employed samples have similar enantiomeric excesses of 60 to 65%, the reported CDs are lower than those of the enantiopure samples by approximately this amount. The antisymmetry of the green curves in Fig. 3 shows that a reversal of the rotation direction of the driving fields has the same effect as changing the handedness of the molecular sample, eliminating the possibility of artifactual contributions. The temporal evolution of $\overline{CD}^{\pm}(n\omega)$ for all harmonic orders is compactly presented in Fig. 4, where the individual images correspond to the points of the pump–probe delay grid.

The CD was first measured in the absence of the pump pulses to characterize the chiral response of the unexcited molecules. The obtained CD is on the order of 2% at H19 (Fig. 3, *Left*) and across the whole range of harmonic orders (Fig. 4*A*). These values are notably smaller than in the case of methyloxirane (27) and limonene (35). Although the CDs were somewhat diminished by the limited enantiopurity of our sample (see above), the CDs should scale approximately linearly with the enantiomeric excess, such that the smallness of the CD must be a property of 2-iodobutane in its electronic ground state.

In the presence of the pump pulses, the CD changed sign and significantly increased in magnitude (Fig. 3) across all detected high-harmonic orders (H10–H31; Fig. 4*B*). At and after time 0 (T_0), the maximal CD values in H19 amounted to 6 to 7%. The averaged $|\overline{CD}^{\pm}(19\omega)|$ value amounted to $\sim$2% at T_0, increased to $\sim$2.5% after 100 fs, and eventually reached a maximum of 2.7% at 250 fs. After 500 fs elapsed, there was essentially no detectable chiral response left, and the same was true for the

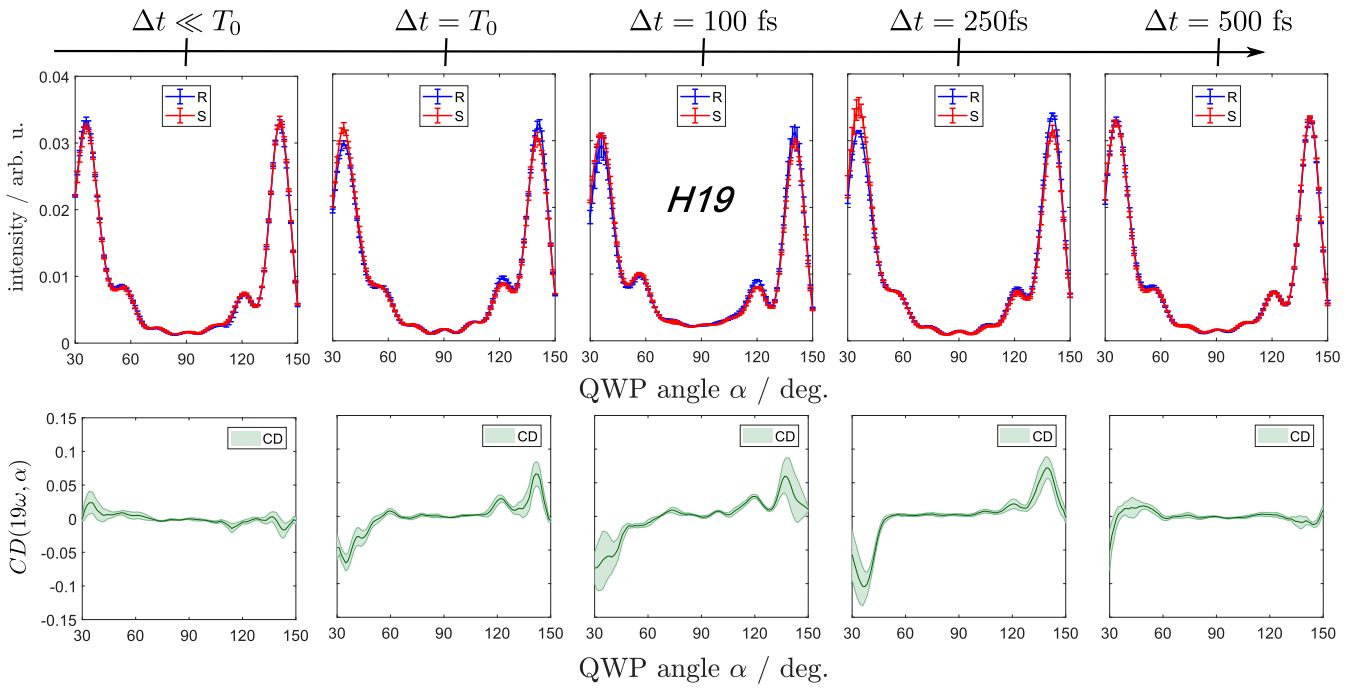

Fig. 3. (*Upper*) Normalized responses of the (*R*) (blue) and the (*S*) (red) enantiomers of 2-iodobutane at different pump–probe delays as a function of ellipticity expressed in terms of the QWP rotation angle α. The signals correspond to H19 of 1,800 nm, or $\sim$ 13.1 eV. (*Lower*) Ellipticity-dependent CD at H19 for each time step. Deg., degree.

subsequent points on the time grid. Other harmonic orders exhibited a qualitatively similar behavior, although there were differences concerning the time delay maximizing the chiral response (see, for instance, H10 and H13 in Fig. 4, for which $|\overline{CD}|$ maximized at $\Delta t = 250$ and 100 fs, respectively).

The results summarized in Fig. 4 lead to the following main conclusions: 1) A strong chiroptical response appears during the excitation by the short 266-nm pulse, which is opposite in sign to that of the unexcited molecules; 2) the induced chiral response persists up to $\gtrsim$250 fs, after which it decays, signaling

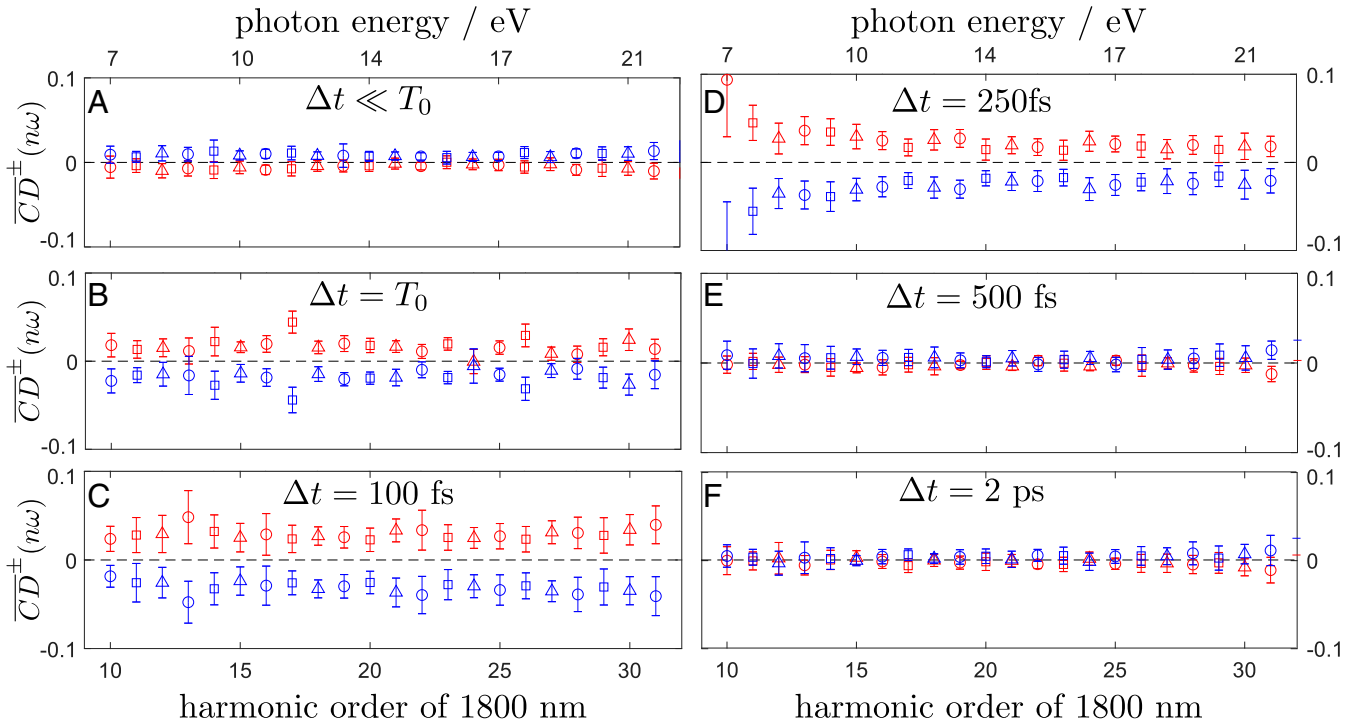

Fig. 4. Ellipticity-averaged CD observed in 2-iodobutane as a function of the photon energy. The data in each image are recorded at a different value of the pump–probe delay Δt.

the formation of an achiral product state; and 3) the chiral response observed below the ionization energy of 2-iodobutane (9.13 eV) displays a strong dependence on the emitted photon energy.

Discussion

In this section, we discuss the experimental observations and provide a qualitative interpretation. There are basically two possible mechanisms for explaining a pump-induced variation of the CD. First, we discuss the role of the rotational dynamics induced by photoexcitation and then proceed with an analysis of the transient CD changes associated with the modifications of the chiral structure of the molecule.

Resonant one-photon excitation leads to the selective excitation of a subensemble of molecules that have their transition-dipole moments aligned along the polarization direction of the pump pulse(s). This effect leads to a partial alignment of the excited molecules that decays on the picosecond time scale. Since CD effects in bicircular HHG strongly depend on the orientation of the molecule relative to the laser field (33), partial alignment can enhance the CDs, and the subsequent rotational dephasing could explain their decay. Therefore, we have performed detailed calculations on the time dependence of the alignment of 2-iodobutane caused by the pump pulses. These calculations, which are summarized in *SI Appendix*, section VI and Fig. S14, show that for typical expected rotational temperatures of 5 to 30 K in our supersonic expansion, the rotational anisotropy decays on a time scale of 11 to 5 ps. Since these time scales are much longer than the observed CD dynamics, we can exclude rotational dynamics as the origin of our observations.

Therefore, the observed CD dynamics are most likely to be caused by the time-dependent evolution of the molecular chirality as the reaction progresses. In the following, we discuss a theoretical model that captures the essential features of the observed chiral dynamics. Our model builds on previous theoretical analysis of bicircular HHG from chiral molecules (26, 27, 48), which has linked the induced chiral response with the interplay of electric- and magnetic-dipole transitions occurring during the propagation of the electron in the continuum. If several valence shells lie sufficiently close in energy ($\lesssim 2$ eV), strong-field ionization can leave the cation in a coherent superposition of several electronic states. During propagation of the electron in the continuum, laser-induced couplings between these states lead to the emergence of HHG "cross-channels," whereby the returning electron recombines with the cation in a state that is different from the one created during ionization. CD emerges through the participation of the weak magnetic-field component of the driving laser pulses in the laser-induced dynamics, whereby the chiral sensitivity is exclusively conveyed by the cross-channels mentioned above. Our previous analysis has shown that, although the corresponding changes in the induced dynamics are extremely small (10^{-4} level in the electron-hole density), a substantial CD (up to 13% in the case of methyloxirane) can result (27).

Limiting our analysis of the Ã-band dynamics to photoexcitation via the ${}^3Q_0^+$ state as explained above, we first extracted the evolution of the expectation value of the C–I-bond distance $[\langle r_{\mathrm{CI}}\rangle(\Delta t)]$ as a function of the pump–probe delay Δt from a wave-packet propagation on the corresponding one-dimensional potential-energy curve (*SI Appendix*, section IV). Within a classical-trajectory treatment, the bond length is bijectively mapped onto the pump–probe delay, which allows us to express all relevant potential-energy curves and coordinate-dependent transition moments as a function of the pump–probe delay. Detailed information on the quantum-chemistry calculations is given in *SI Appendix*, section III.

Considering the pulse intensities employed in the experiment ($\lesssim 5\times10^{13}\,\mathrm{W/cm^2}$ and wavelengths of 1,800/900 nm), strong-field ionization from the ${}^3Q_0^+$ state populates mainly the ground ($\tilde{X}^+$, split into two spin-orbit components with vertical ionization potentials I_{p} of ≈ 9.13 and ≈ 9.68 eV) and the first excited ($\tilde{A}^+$, $I_{\mathrm{p}} \approx 11.08$ eV) states (49, 50). Neglecting the spin-orbit interaction in the cationic states, this gives rise to in total four channels contributing to the HHG process. Two channels are formed by strong-field ionization to the $\tilde{X}^+$ or $\tilde{A}^+$ state of the cation and photorecombination of the continuum electron with the same state. These channels are accordingly labeled XX or AA. In addition, there are two "cross-channels" (XA and AX). Under these premises, the treatment of the laser-induced dynamics reduces to a system of two coupled ordinary differential equations that has a straightforward solution, as presented in *SI Appendix*, section V. After integrating *SI Appendix*, Eq. **S5** over the duration $\overline{\tau}_{IJ}^{\Omega}$ of a given electron trajectory (typical values ranging from 1.4 to 1.8 fs for our experimental conditions), the calculated coefficients $\{c_{IJ}(\Delta t)\}$ (with $\{I,J\}\in\{X,A\}$) for each channel are used to obtain the frequency-domain HHG dipole response (at a photon energy Ω) as a function of the pump–probe delay (26):

$$\mathbf{d}(\Omega,\Delta t) = \sum_{IJ} c_{IJ}(\Delta t)\, a_{ion}^{I}(\Omega,\Delta t)\left(\frac{2\pi}{i\overline{\tau}_{IJ}^{\Omega}(\Delta t)}\right)^{(3/2)} e^{iS(\Omega,\overline{\tau}_{IJ}^{\Omega})} \times \mathbf{a}_{rec}^{J}(\Delta t), \qquad [2]$$

where $S(\Omega,\overline{\tau}_{IJ}^{\Omega})$ corresponds to the semiclassical action.

Here, we are primarily interested in rationalizing the temporal profile of the chiral response, as a complete quantitative description of the HHG process for many-electron systems is still out of reach. Therefore, we set the ionization $[a_{ion}^{I}(\Omega,\Delta t)]$ and the recombination $[\mathbf{a}_{rec}^{J}(\Omega,\Delta t)]$ matrix elements in Eq. **2** to unity, which amounts to neglecting their dependence on the ionization/recombination directions in the molecular frame. With these approximations, the chiral response is entirely encoded in the variation of the electric- and magnetic-dipole matrix elements within the subcycle temporal interval between ionization and recombination. The time-dependent CD $CD(\Omega,\Delta t)$ is estimated by calculating the spectral HHG intensity $\tilde{S}(\Omega;\Delta t)\propto|\mathbf{d}(\Omega,\Delta t)|^2$ for a (R)-2-iodobutane molecule with its C–I-bond axis aligned along the instantaneous electric-field direction as well as for its (S)-enantiomer and subsequently forming the differential response:

$$CD(\Omega,\Delta t) = 2\frac{\tilde{S}^{(R)}(\Omega,\Delta t)-\tilde{S}^{(S)}(\Omega,\Delta t)}{\max\left(\tilde{S}^{(R)}(\Omega,\Delta t)+\tilde{S}^{(S)}(\Omega,\Delta t)\right)}. \qquad [3]$$

Fig. 5 shows the CD obtained with the above relation for three selected harmonic orders ($H16$, $H20$, and $H31$) as a function of the pump–probe delay. Since our model does not contain the structure-sensitive contributions from the ionization and the recombination steps, a quantitative prediction of the magnitude of $\overline{CD}^{\pm}(\Omega)$ is not expected.

However, a special feature of our HHG scheme of probing chiral dynamics is the fact that the chiroptical response entirely originates from the second, continuum-propagation step, in which the electron can be treated as decoupled from the parent ion in good approximation. Therefore, the time dependence of the chiral response will mainly be dictated by the variation of the chiral structure of the probed molecule, which is encoded in the geometry-dependent electric and magnetic dipole-transition-matrix elements of the cation. In our work, the latter are calculated with high accuracy

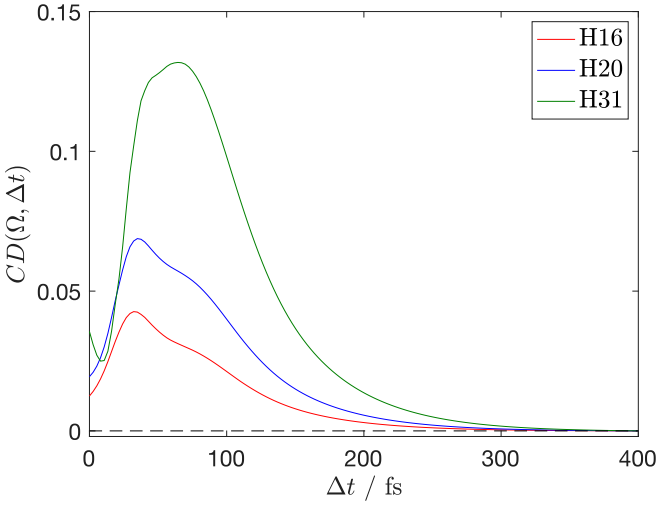

Fig. 5. Time-dependent CD signal, evaluated according to Eq. **3** at photon energies corresponding to *H*16, *H*20, and *H*31 of 1,800 nm. The instantaneous direction of the ionizing bicircular field is set parallel to the C–I-bond axis. The signal is averaged over the azimuthal angle associated with this axis.

by using modern quantum-chemistry methods (*SI Appendix*, section III).

Our results predict a rapid increase of the CD signal at early time delays, followed by one relatively sharp local maximum around 30–40 fs, a broad shoulder feature around 80–90 fs, followed by a monotonous decay by two to three orders of magnitude within ∼250 to 300 fs. The overall dynamics of the calculated CDs therefore capture the main features of the experimental results, which show local maxima around 100 fs and a subsequent decay. Moreover, the results in Fig. 5 predict a pronounced spectral dependence of the time-dependent chiral response, which is also present in the experimental results shown in Fig. 4. This comparison shows that our simple model captures the salient features of the measured chiral dynamics. Our calculations further allow us to conclude that the decay of the chiral response and its vanishing for long delays reflect the progressive loss of chirality during the C–I-bond-breaking process. We have carried out a detailed comparison of the predictions of our theoretical model, including or neglecting the planarization of the 2-butyl radical (*SI Appendix*, section III B). This comparison has shown that the geometric relaxation of the 2-butyl radical does not qualitatively change the predicted CD dynamics, which are therefore dominated by the detachment of the iodine atom from the molecular backbone. The observed disappearance of the CD therefore reflects the loss of chirality of the dissociating system as a whole during its transformation into fragments that are achiral on their own. This conclusion is further supported by our analysis of the potential-energy surface of the 2-butyl radical along the internal coordinate that interconverts its two enantiomers. The calculations presented in *SI Appendix*, section VIII corroborate the fact that the vibrational zero-point level lies above the barrier separating the two enantiomers and therefore corresponds to an achiral equilibrium geometry.

Turning to the remaining discrepancies, we note that the measured CDs appeared to decay more slowly than the calculated ones. Similarly, we noted above that the (nonchiral) signals suggest a longer dissociation time (340 fs) than predicted by our one-dimensional wave-packet calculations. The consistent deviation of these two classes of observables from their calculated counterparts most likely originates from neglecting the structure-dependent ionization and recombination matrix elements, because all other quantities have been accurately incorporated into our theoretical model.

Conclusion

In this article, we have introduced a technique for detecting time-dependent chirality during a chemical reaction. We have applied this technique to study the chirality changes occurring in the course of the photodissociation of 2-iodobutane. With the aid of a conceptually simple theoretical treatment based on high-level ab initio quantum-chemical calculations, we have been able to correlate the time evolution of the CD signal with the coordinate dependence of the electric- and magnetic-dipole matrix elements that encode the chiral response in the HHG process.

This technique is sufficiently sensitive to be applicable to the gas phase, but is equally applicable to liquids (42) and solids (39) in future experiments. Its relatively large CD effects, comparable in magnitude to PECD, combined with its all-optical nature make it a powerful chiral-sensitive method for detecting ultrafast changes in molecular chirality. The ability to probe chiral photochemical processes on such time scales opens up a variety of possibilities for investigating chiral-recognition phenomena, such as the processes that determine the outcome of enantioselective chemical reactions. Paired with recent developments in condensed-phase high-harmonic spectroscopy, our technique will rapidly be applied to all phases of matter, where it will unlock the study of a range of chiral phenomena on ultrashort time scales.

Methods

Details on the experimental setup and data evaluation are given in *SI Appendix*, section I. The synthesis of enantiomerically enriched 2-iodobutane is described in *SI Appendix*, section II. The theoretical work, including the quantum-chemical ab initio calculations, the quantum-dynamical calculations, and the CD calculations, is given in *SI Appendix*, sections III–VIII.

Data Availability. The data presented in this article are available from the corresponding author upon request.

ACKNOWLEDGMENTS. D.B. thanks Prof. Frank Neese for helpful discussions regarding the calculation of the distance-dependent magnetic dipole moments. We thank ETH Zurich for the allocation of computational resources on the EULER cluster. We thank Prof. Ivan Powis (Nottingham) for suggesting to study 2-iodobutane in this work. This work was supported by Swiss National Science Foundation Project 200021_172946 and the National Center of Competence in Research–Molecular Ultrafast Science and Technology.

1. D. E. Frantz, R. Fässler, E. M. Carreira, Facile enantioselective synthesis of propargylic alcohols by direct addition of terminal alkynes to aldehydes. *J. Am. Chem. Soc.* **122**, 1806–1807 (2000).
2. T. P. Yoon, E. N. Jacobsen, Privileged chiral catalysts. *Science* **299**, 1691–1693 (2003).
3. K. W. Quasdorf, L. E. Overman, Catalytic enantioselective synthesis of quaternary carbon stereocentres. *Nature* **516**, 181–191 (2014).
4. J. Meyer-Ilse, D. Akimov, B. Dietzek, Recent advances in ultrafast time-resolved chirality measurements: Perspective and outlook. *Laser Photon. Rev.* **7**, 495–505 (2013).
5. M. Bonmarin, J. Helbing, A picosecond time-resolved vibrational circular dichroism spectrometer. *Opt. Lett.* **33**, 2086–2088 (2008).
6. H. Rhee *et al.*, Femtosecond characterization of vibrational optical activity of chiral molecules. *Nature* **458**, 310–313 (2009).
7. C. Niezborala, F. Hache, Measuring the dynamics of circular dichroism in a pump-probe experiment with a Babinet-Soleil compensator. *J. Opt. Soc. Am. B* **23**, 2418–2424 (2006).
8. D. Abramavicius, S. Mukamel, Time-domain chirally-sensitive three-pulse coherent probes of vibrational excitons in proteins. *Chem. Phys.* **318**, 50–70 (2005).
9. F. Hache *et al.*, Picosecond transient circular dichroism of the photoreceptor protein of the light-adapted form of Blepharisma japonicum. *Chem. Phys. Lett.* **483**, 133–137 (2009).
10. J. Meyer-Ilse, D. Akimov, B. Dietzek, Ultrafast circular dichroism study of the ring opening of 7-dehydrocholesterol. *J. Phys. Chem. Lett.* **3**, 182–185 (2012).
11. M. Oppermann *et al.*, Ultrafast broadband circular dichroism in the deep ultraviolet. *Optica* **6**, 56–60 (2019).

12. J. R. Rouxel, M. Kowalewski, S. Mukamel, Photoinduced molecular chirality probed by ultrafast resonant x-ray spectroscopy. *Struct. Dyn.* **4**, 044006 (2017).
13. Y. Zhang, J. R. Rouxel, J. Autschbach, N. Govind, S. Mukamel, X-ray circular dichroism signals: A unique probe of local molecular chirality. *Chem. Sci.* **8**, 5969–5978 (2017).
14. J. R. Rouxel, Y. Zhang, S. Mukamel, X-ray Raman optical activity of chiral molecules. *Chem. Sci.* **10**, 898–908 (2019).
15. M. Quack, Structure and dynamics of chiral molecules. *Angew Chem. Int. Ed. Engl.* **28**, 571–586 (1989).
16. D. Patterson, M. Schnell, J. M. Doyle, Enantiomer-specific detection of chiral molecules via microwave spectroscopy. *Nature* **497**, 475–477 (2013).
17. P. Herwig *et al.*, Imaging the absolute configuration of a chiral epoxide in the gas phase. *Science* **342**, 1084–1086 (2013).
18. M. Pitzer *et al.*, Direct determination of absolute molecular stereochemistry in gas phase by Coulomb explosion imaging. *Science* **341**, 1096–1100 (2013).
19. R. Li, R. Sullivan, W. Al-Basheer, R. M. Pagni, R. N. Compton, Linear and nonlinear circular dichroism of R-(+)-3-methylcyclopentanone. *J. Chem. Phys.* **125**, 144304 (2006).
20. A. Bornschlegl, C. Logé, U. Boesl, Investigation of CD effects in the multi photon ionisation of R-(+)-3-methylcyclopentanone. *Chem. Phys. Lett.* **447**, 187–191 (2007).
21. B. Ritchie, Theory of the angular distribution of photoelectrons ejected from optically active molecules and molecular negative ions. *Phys. Rev. A* **13**, 1411–1415 (1975).
22. N. Böwering *et al.*, Asymmetry in photoelectron emission from chiral molecules induced by circularly polarized light. *Phys. Rev. Lett.* **86**, 1187–1190 (2001).
23. I. Powis, Photoelectron circular dichroism in gas phase chiral molecules. *Adv. Chem. Phys.* **138**, 267–329 (2008).
24. A. Ferré *et al.*, A table-top ultrashort light source in the extreme ultraviolet for circular dichroism experiments. *Nat. Photon.* **9**, 93–98 (2014).
25. S. Beaulieu *et al.*, Universality of photoelectron circular dichroism in the photoionization of chiral molecules. *New J. Phys.* **18**, 102002 (2016).
26. R. Cireasa *et al.*, Probing molecular chirality on a sub-femtosecond timescale. *Nat. Phys.* **11**, 654–658 (2015).
27. D. Baykusheva, H. J. Wörner, Chiral discrimination through bielliptical high-harmonic spectroscopy. *Phys. Rev. X* **8**, 031060 (2018).
28. A. Comby *et al.*, Relaxation dynamics in photoexcited chiral molecules studied by time-resolved photoelectron circular dichroism: Toward chiral femtochemistry. *J. Phys. Chem. Lett.* **7**, 4514–4519 (2016).
29. H. J. Wörner, J. B. Bertrand, D. V. Kartashov, P. B. Corkum, D. M. Villeneuve, Following a chemical reaction using high-harmonic interferometry. *Nature* **466**, 604–607 (2010).
30. H. J. Wörner *et al.*, Conical intersection dynamics in NO_2 probed by homodyne high-harmonic spectroscopy. *Science* **334**, 208–212 (2011).
31. P. M. Kraus *et al.*, Time-resolved high-harmonic spectroscopy of nonadiabatic dynamics in NO_2. *Phys. Rev. A* **85**, 043409 (2012).
32. O. Smirnova, Y. Mairesse, S. Patchkovskii, Opportunities for chiral discrimination using high harmonic generation in tailored laser fields. *J. Phys. B At. Mol. Opt. Phys.* **48**, 234005 (2015).
33. D. Ayuso, P. Decleva, S. Patchkovskii, O. Smirnova, Chiral dichroism in bi-elliptical high-order harmonic generation. *J. Phys. B At. Mol. Opt. Phys.* **51**, 06LT01 (2018).
34. D. Ayuso, P. Decleva, S. Patchkovskii, O. Smirnova, Strong-field control and enhancement of chiral response in bi-elliptical high-order harmonic generation: An analytical model. *J. Phys. B At. Mol. Opt. Phys.* **51**, 124002 (2018).
35. Y. Harada, E. Haraguchi, K. Kaneshima, T. Sekikawa, Circular dichroism in high-order harmonic generation from chiral molecules. *Phys. Rev. A* **98**, 021401 (2018).
36. S. Baker *et al.*, Probing proton dynamics in molecules on an attosecond time scale. *Science* **312**, 424–427 (2006).
37. H. J. Wörner, H. Niikura, J. B. Bertrand, P. B. Corkum, D. M. Villeneuve, Observation of electronic structure minima in high-harmonic generation. *Phys. Rev. Lett.* **102**, 103901 (2009).
38. P. M. Kraus *et al.*, Measurement and laser control of attosecond charge migration in ionized iodoacetylene. *Science* **350**, 790–795 (2015).
39. S. Ghimire *et al.*, Observation of high-order harmonic generation in a bulk crystal. *Nat. Phys.* **7**, 138–141 (2011).
40. T. T. Luu *et al.*, Extreme ultraviolet high-harmonic spectroscopy of solids. *Nature* **521**, 498–502 (2015).
41. G. Vampa *et al.*, Linking high harmonics from gases and solids. *Nature* **522**, 462–464 (2015).
42. T. T. Luu, et al., Extreme-ultraviolet high-harmonic generation in liquids. *Nat. Commun.* **9**, 3723 (2018).
43. A. Gedanken, The magnetic circular dichroism of the *A* band in CF_3I, C_2H_5I and *t*-BuI. *Chem. Phys. Lett.* **137**, 462–466 (1987).
44. Y. Mairesse *et al.*, High-order harmonic transient grating spectroscopy in a molecular jet. *Phys. Rev. Lett.* **100**, 143903 (2008).
45. J. B. Bertrand *et al.*, Ultrahigh-order wave mixing in noncollinear high harmonic generation. *Phys. Rev. Lett.* **106**, 023001 (2011).
46. M. E. Corrales *et al.*, Structural dynamics effects on the ultrafast chemical bond cleavage of a photodissociation reaction. *Phys. Chem. Chem. Phys.* **16**, 8812 (2014).
47. A. Tehlar, H. J. Wörner, Time-resolved high-harmonic spectroscopy of the photodissociation of CH_3I and CF_3I. *Mol. Phys.* **111**, 2057–2067 (2013).
48. O. Smirnova, Y. Mairesse, S. Patchkovskii, Opportunities for chiral discrimination using high harmonic generation in tailored laser fields. *J. Phys. B At. Mol. Opt. Phys.* **48**, 234005 (2015).
49. R. G. Dromey, J. B. Peel, Photoelectron spectroscopic correlation of the molecular orbitals of the alkanes and alkyl iodides. *J. Mol. Struct.* **23**, 53–64 (1974).
50. K. Kimura, S. Katsumata, Y. Achiba, T. Yamazaki, S. Iwata, *Handbook of HeI Photoelectron Spectra of Findamental Organic Molecules* (Japan Scientific Society Press, Tokyo, 1981).